Faraday Discussions

Accepted Manuscript

This manuscript will be presented and discussed at a forthcoming Faraday Discussion meeting. All delegates can contribute to the discussion which will be included in the final volume.

Register now to attend! Full details of all upcoming meetings: http://rsc.li/fd-upcoming-meetings

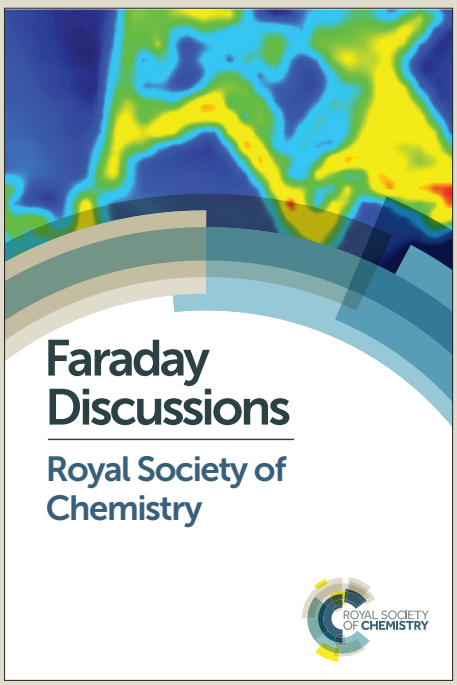

This is an *Accepted Manuscript*, which has been through the Royal Society of Chemistry peer review process and has been accepted for publication.

Accepted Manuscripts are published online shortly after acceptance, before technical editing, formatting and proof reading. Using this free service, authors can make their results available to the community, in citable form, before we publish the edited article. We will replace this *Accepted Manuscript* with the edited and formatted *Advance Article* as soon as it is available.

You can find more information about *Accepted Manuscripts* in the Information for Authors.

Please note that technical editing may introduce minor changes to the text and/or graphics, which may alter content. The journal's standard Terms & Conditions and the Ethical guidelines still apply. In no event shall the Royal Society of Chemistry be held responsible for any errors or omissions in this *Accepted Manuscript* or any consequences arising from the use of any information it contains.

ROYAL SOCIETY OF CHEMISTRY

www.rsc.org/faraday_d

Journal Name

RSCPublishing

ARTICLE

Determination of a Localized Surface Plasmon Resonance Mode of Cu_7S_4 Nanodisks by Plasmon Coupling

Cite this: DOI: 10.1039/x0xx00000x

Received ooth January 2012,
Accepted ooth January 2012

DOI: 10.1039/x0xx00000x

www.rsc.org/

L. Chen,[a] M. Sakamoto,[bc] R. Sato[b] and T. Teranishi[*b]

Plasmon properties such as peak position, extinction cross-section, and local electric field intensity, are strongly dependent on excited, localized surface plasmon resonance (LSPR) modes. In non-spherical copper chalcogenide nanoparticles, assignment of the LSPR peaks to the corresponding oscillation modes has been controversial and requires experimental verification. We determined the in-plane LSPR mode of roxbyite Cu_7S_4 nanodisks from the plasmon coupling effect of nanodisks in solution. Compared with individual Cu_7S_4 nanodisks, self-assembled Cu_7S_4 nanodisk arrays in chloroform exhibited a blue-shifted LSPR peak with weaker optical density. This strongly suggests that the singular LSPR peak in the near-infrared region mainly originates from the in-plane oscillation mode. In addition, we demonstrate that the same LSPR peak can be readily tuned by controlling the number of disks in the array.

Introduction

Localized surface plasmon resonance (LSPR) is a collective oscillation of free carriers in resonance with incident light. At the LSPR frequency, the absorption cross-section, scattering cross-section, and local electric field intensity are significantly enhanced.[1] The LSPR of metal nanoparticles (NPs) can be finely tuned through manipulation of composition, size, and shape, as well as the refractive index of the surrounding medium.[2] As a result of the unique optical and electrical properties of LSPR, plasmonic NPs have stimulated a wide range of applications including photothermal therapy,[3] surface-enhanced Raman scattering,[4] metal-enhanced fluorescence,[5] and phtocatalysis.[6] LSPR emerges not only in metals but also in semiconductors that have appreciable carrier density. Because they have a much lower carrier density (~10^{21} cm^{-3}) relative to metals (~10^{23} cm^{-3}), semiconductors exhibit LSPR responses in the near-infrared (NIR) and mid-infrared (MIR) regions.[7,8,9] This is understood from the relation:

$$\omega_p = \sqrt{\frac{N_h e^2}{\varepsilon_0 m_h}}$$

where ω_p is the bulk plasma frequency, N_h is the density of free carriers, e is the electron charge, and m_h is the hole effective mass. The advantages of LSPR in *p*-type semiconductors ($Cu_{2-x}S$, $Cu_{2-x}Se$) are controllable responses *via* carrier density, oxidative generation, and reductive filling of copper vacancies.[10] In metal NPs, once the size, shape, or the refractive index of the surrounding medium is fixed, the LSPR response is locked and cannot be dynamically tuned.[7] Another advantage over metallic NPs is the existence of various $Cu_{2-x}S$ and $Cu_{2-x}Se$ NP crystal structures. For example, in $Cu_{2-x}S$ NPs, the degree of copper deficiency (x) varies in a wide range between 0 and 1, from the Cu-abundant Cu_2S phase (chalcocite) to the Cu-poor CuS phase (covellite).[11] $Cu_{2-x}S$ NPs with different crystal structures exhibit unique LSPR responses. Djurleite $Cu_{1.96}S$ nanodisks have two distinct LSPR peaks in the NIR and MIR regions,[12] while covellite CuS nanodisks have only one peak in the NIR region.[13] Carrier density and crystal structure control of $Cu_{2-x}S$, $Cu_{2-x}Se$ NPs are good ways to investigate LSPR responses beyond metals. Because of the unique LSPR properties, $Cu_{2-x}S$, $Cu_{2-x}Se$ NPs have potential applications in bio-imaging, photothermal therapy,[14,15] and NIR optical switching[16].

Assignment of an LSPR peak to a corresponding oscillation mode is important for a better understanding of LSPR and its applications. However, this has been a challenge for copper chalcogenide NPs. The LSPR response of non-spherical gold and silver nanorods can be reproduced with numerical simulations such as the discrete dipole approximation or finite difference time domains.[17] In contrast, numerical simulations cannot be applied to copper chalcogenides. For example, Feldmann et al. reported that the Drude model could not describe the LSPR responses well in $Cu_{2-x}X$ (X=S, Se, Te) NPs, because the free holes in the $Cu_{2-x}X$ valance band cannot be viewed as full free carriers, and the effects of hole localization need to be taken into consideration. In addition, the empirical dielectric function determined from thin films cannot be directly used to analyze the LSPR responses.[18,19]

Several experimental approaches could be used to assign LSPR peaks of $Cu_{2-x}S$ nanodisks to corresponding oscillation modes. With an increasing aspect ratio AR (diameter/thickness), the in-plane LSPR peak of silver nanodisks is expected to be red-shifted, while the out-of-plane peak is expected to be blue-shifted.[20] In contrast, an in-plane LSPR peak shift for $Cu_{2-x}S$ nanodisks with increasing AR is not observed, while the in-plane LSPR peak for $Cu_{1.96}S$ nanodisks is blue-shifted with increasing AR because of the increased

carrier density.[12] Finally, the in-plane LSPR peak of the CuS nanodisk is red-shifted with increasing AR.[13] Thus, assignment of LSPR peaks is not possible by simply increasing the ARs of the $Cu_{2-x}S$ nanodisks. Interaction between excited LSPR modes in solution (plasmon coupling) can be used to assign a $Cu_{2-x}S$ nanodisk LSPR peak to the corresponding oscillation mode. This is because when the NPs are assembled with small gaps between the disks, plasmon coupling between excited LSPR modes induces significant LSPR changes such as peak position, extinction cross section, and local electric field intensity.[21] Thus, it is possible to determine the excited LSPR mode from the plasmon coupling. For example, compared with single $Cu_{2-x}S$ nanodisks, the in-plane plasmon coupling of face-to-face assembled $Cu_{2-x}S$ nanodisks is expected to induce a blue shift of the LSPR peak and a decrease in optical density. Conversely, the out-of-plane plasmon coupling of face-to-face assembled $Cu_{2-x}S$ nanodisks is expected to induce a red shift of the LSPR peak and an increase in optical density. By way of this difference, one can assign the observed LSPR peak to the corresponding oscillation mode experimentally.

Here, we synthesized high-quality roxbyite Cu_7S_4 nanodisks as described previously,[22] and assigned the LSPR peak in the NIR region to the corresponding oscillation mode. To induce plasmon coupling, column-like Cu_7S_4 nanodisk arrays are fabricated *via* ligand replacement of oleylamine (OAm) with 1-dodecanethiol (1-DT). The formation of Cu_7S_4 nanodisk arrays in $CHCl_3$ is investigated through real-time dynamic light scattering (DLS) and ^{1}H-NMR. From LSPR spectral shifts during nanodisk array formation, we conclude that the singular LSPR peak in the NIR region resulted mainly from the in-plane oscillation mode. In addition, we demonstrate that the number of disks can finely control the LSPR properties of the Cu_7S_4 arrays.

Experimental

Chemicals.

Oleylamine (OAm, 80–90%) and *N*,*N*-dibutylthiourea (DBTU, 97%) were purchased from Acros Organics. The DBTU was used as received, while the OAm was first distilled under vacuum. Copper stearate ($Cu[CH_3(CH_2)_{16}COO]_2$, >8.0% as Cu) was purchased from Kanto Chemicals. Diisobutyl aluminum hydride toluene solution (DIBAH, 1.5 mol/L), 1-dodecanethiol ($C_{12}H_{25}SH$, 98.0%), ethanol (99.5%), toluene, and chloroform were purchased from Wako Chemicals. The oxygen (O_2) dissolved in OAm, ethanol, toluene, and chloroform was removed *via* repeated freeze-pump-thaw cycles. The other chemicals were used as received.

Synthesis of Cu_7S_4 nanodisks.

The synthesis of Cu_7S_4 nanodisks was performed as described previously.[22] In a typical O_2-free synthesis, copper stearate (1.89 g, 3.0 mmol), DBTU (1.12 g, 6.0 mmol), and O_2-free oleylamine (6 mL) were added to a 100-mL glass tube and heated to 80 °C at the rate of 10 °C/min under N_2 while stirring. After further stirring at 80 °C for 1 h, the mixture was cooled to room temperature. The sample was then moved into an argon-filled glove box and transferred to a centrifuge tube. After centrifugation with O_2-free toluene/ethanol (v/v=1:3), the precipitate was dispersed in O_2-free toluene or chloroform and stored in the glove box. The average yield of Cu_7S_4 nanodisks was 95%.

Ligand exchange of Cu_7S_4 nanodisks.

The ligand exchange in Cu_7S_4 nanodisks from OAm to 1-DT is based on hard-soft acid-base theory. The affinity between copper and sulfur in 1-DT is stronger than the affinity between copper and nitrogen in OAm. Briefly, a desired amount of 1-DT was rapidly injected into 5 mL of oxidized Cu_7S_4 nanodisks (5.1 nmol) in $CHCl_3$ and then sonicated under N_2 for 30 min. Ultraviolet-visible (UV-vis)-NIR absorption spectra were recorded immediately afterward.

Characterization.

Transmission electron microscopy (TEM) was performed with a JEM-1011 (JEOL) at an accelerating voltage of 100 kV. The thicknesses and diameters of the synthesized Cu_7S_4 nanodisks were determined by measuring several hundred disks in the TEM images. Scanning electron microscopy (SEM) images were acquired with a field emission S-4800 (FE-SEM, Hitachi) at an accelerating voltage of 5 kV. All the air-sensitive samples were dried in a glove box. UV-vis-NIR (300 − 2500 nm) absorption spectra of synthesized Cu_7S_4 nanodisks were acquired in a 1-mm quartz cuvette in a U-4100 spectrophotometer (Hitachi). Oxidation was prevented before and during the measurement by tightly sealing the quartz cuvette. Fourier transform infrared spectra were acquired with an IRPrestige-21 (Shimadzu). Photoluminescence analysis was performed with a Fluorolog-3 Model:TTT6 (Nanolog). Cu_7S_4 nanodisks were excited at 400 nm, and the 1-cm quartz cuvette was tightly sealed to prevent oxidation. X-ray diffraction (XRD) patterns of oxidized Cu_7S_4 nanodisks were acquired on a X'Pert Pro MPD (PANalytical) with CuKα radiation (λ=1.542 Å) at 45 kV and 40 mA. DLS measurements to monitor the size variation of the Cu_7S_4 nanodisk arrays in $CHCl_3$ were performed with an ELS-ZA2 (Otsuka Electronics). To determine the surface-capping agent of the Cu_7S_4 nanodisks, 1H-NMR was acquired with a 200-MHz Varian Gemini 200 NMR spectrometer.

Results and discussion

Morphologies and optical properties of Cu_7S_4 nanodisks.

High-quality Cu_7S_4 nanodisks were synthesized using DBTU as the sulfur source. Figure 1a and b shows SEM and TEM images, respectively of the Cu_7S_4 nanodisks. Because of their uniform size (diameter: 14.0±1.0 nm, thickness: 4.5±0.5 nm) and shape, the nanodisks stack in a layer-by-layer fashion on the Si substrate. The obtained Cu_7S_4 nanodisks were found to have a triclinic roxbyite structure from an XRD measurement (Fig. S1). Figure 1c shows a strong LSPR absorption peak for the Cu_7S_4 nanodisks that derives from collective free-hole oscillations generated by excess copper vacancies in the valence band. OAm forms a complex with copper ions, which may generate the copper vacancies in the NPs during nucleation and growth.[23] Alivisatos et al. reported the synthesis of stoichiometric Cu_2S NPs without OAm, and the non-oxidized Cu_2S NPs exhibited no LSPR absorption band.[24] Therefore, OAm-induced vacancies led to the LSPR absorption in our nanodisks. Previous studies have shown that freshly synthesized Cu_2S NPs were easily oxidized and reduced.[7,10] Oxidative agents including oxygen[7], iodine[23], and the Ce(IV) complex[25] can induce the creation of copper vacancies in the Cu_2S lattice, leading to an increase in carrier density. In UV-vis-NIR spectra, oxidation causes a blue shift in the LSPR peak,

increases the absorption intensity, narrows the line width, and increases the onset of absorption. Conversely, reductive agents including DIBAH[10], thiols,[23] and Cu(I) salts[25] induce the filling of copper vacancies in the $Cu_{2-x}S$ lattice, leading to a decrease in carrier density. The reduction causes a red shift in the LSPR peak, decreases the absorption intensity, broadens the line width, and decreases the onset of the absorption band. The oxidation of Cu_7S_4 nanodisks by air, reduction by DIBAH, and re-oxidation by air is displayed in Figures S2 and S3. All the Cu_7S_4 nanodisk spectral shifts and variations in optical density were consistent with previous reports.[7,10]

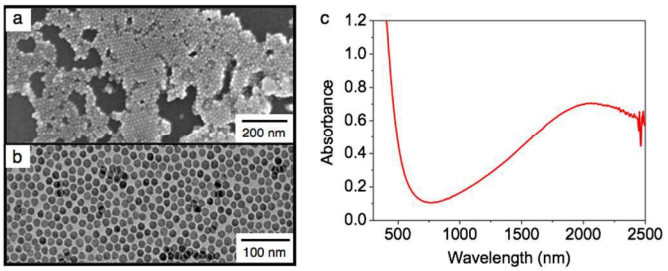

Fig. 1 (a) SEM and (b) TEM images of Cu_7S_4 nanodisks. (c) UV-vis-NIR spectrum of Cu_7S_4 nanodisks in toluene before oxidation.

Formation of Cu_7S_4 nanodisk arrays.

Face-to-face contacts, with narrow inter-disk spaces in the arrays, enable plasmon coupling between the Cu_7S_4 nanodisks. From the UV-vis-NIR spectral shift caused by array formation, we can assign the Cu_7S_4 nanodisk LSPR peak in the NIR region to the corresponding oscillation mode. Previously, Tao et al. reported that 1-DT-capped $Cu_{2-x}S$ nanodisks formed Langmuir-Blodgett films of nanodisk arrays.[19] Hence, we developed a convenient and versatile method for forming one-dimensional nanodisk arrays in solution. The Cu_7S_4 nanodisk arrays were fabricated *via* ligand exchange of OAm-Cu_7S_4 nanodisks (5.1 nmol) by sonication with 1-DT (80 µmol) in $CHCl_3$ (5 mL) under N_2. TEM and SEM images of the arrays are in Figure S4. Strong intermolecular interaction among the 1-DT was responsible for the column-like structures. To investigate the growth and length distribution of the Cu_7S_4 nanodisk arrays in $CHCl_3$, we conducted real-time DLS measurements. As shown in Figure 2a, long Cu_7S_4 nanodisk arrays initially formed after addition of 1-DT and sonication. Time-resolved TEM images in Figure 2b reveal the co-existence of isolated nanodisks and nanodisk arrays with various lengths, 20 min after the 1-DT addition. The isolated Cu_7S_4 nanodisks gradually attached to the nanodisk arrays, increasing their length. After 3.5 h, the isolated nanodisks were rarely observed, and most of the arrays were 18–130 nm long and were precipitated. It should be noted that sonication aids the extent or the rate of ligand exchange, which leads to the formation of the Cu_7S_4 nanodisk arrays. In the absence of sonication, Cu_7S_4 nanodisks were merely reduced by the 1-DT (Figure S5). This is consistent with Alivisatos et al.,[23] who suggested that the reduction involved either disulfide formation or the coordination of thiol molecules to copper atoms on the NP surface.

$Cu_{1.96}S$ nanodisks capped with 1-DT are likely to form arrays because of the strong hydrophobic interactions among 1-DT molecules.[12] Similarly, Cu_7S_4 nanodisks self-assemble into arrays when the initial OAm surfactant is replaced with 1-DT. To confirm that ligand exchange, ^{1}H-NMR spectra were acquired (Figure 3a). After the addition of 1-DT and sonication, the 5.38-ppm chemical shift of the OAm alkene H disappeared, and the 2.67-ppm shift of the methylene H next to the 1-DT sulfanyl group appeared. Thus, OAm molecules on the surface of the Cu_7S_4 nanodisks were replaced by 1-DT molecules. Relative to the spectra of free OAm and 1-DT molecules in $CDCl_3$, the broadened peaks in both samples are attributed to surface interactions on the nanodisks.[26] In addition, the TEM images in Figure 2b reveal that the inter-particle distance (~2.2 nm) is shorter than twice the molecular length of 1-DT (2×1.6 nm), indicating that inter-penetration among linear 1-DT molecules on the nanodisks induces strong hydrophobic interactions. The latter enables face-to-face self-assembly of growing Cu_7S_4 nanodisks arrays with time. In contrast, the non-linear cis-conformation of OAm leads to a strong steric repulsion that prevents face-to-face self-assembly of the nanodisks. Thus, OAm capped nanodisks are dispersed in $CHCl_3$ and no arrays are observed.

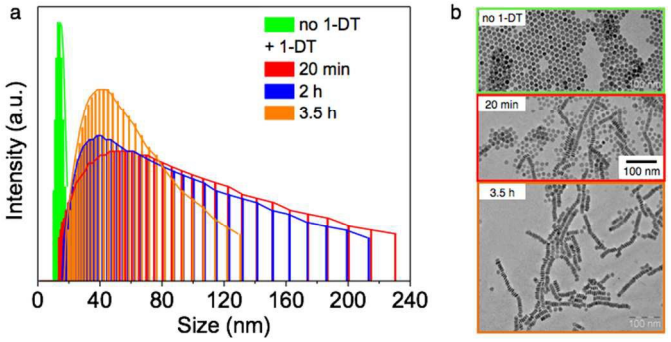

Fig. 2 (a) Time evolution of DLS spectra recorded after addition of 1-DT (80 µmol) to oxidized Cu_7S_4 nanodisks in $CHCl_3$ (5 mL) (final 1-DT conc. = 16.2 mM), and then sonication under N_2 for 30 min. (b) TEM images of Cu_7S_4 nanodisks and nanodisk arrays for growth time at 20 min and 3.5 h.

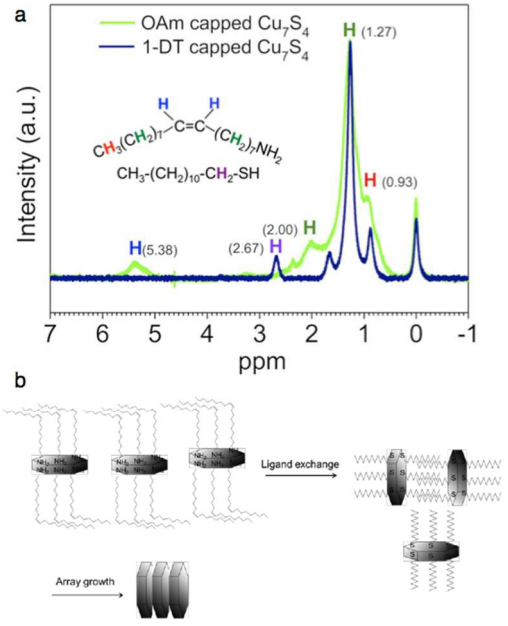

Fig. 3 (a) ^{1}H-NMR spectra of OAm and 1-DT capped Cu_7S_4 nanodisks. Inset: chemical structures of OAm and 1-DT molecules. (b) Proposed mechanism for the formation of Cu_7S_4 nanodisk arrays.

Assignment of LSPR mode in NIR region.

Because of the 2.2-nm inter-particle distance in the Cu_7S_4 nanodisk arrays, a strong near-field coupling is expected. By comparing the LSPR properties between the isolated Cu_7S_4 nanodisks and the arrays, we can determine the LSPR mode in the NIR region. Figure 4a plots the time evolution of UV-vis-NIR nanodisk spectra after the addition of 1-DT. The LSPR peak is gradually blue-shifted, while the optical density gradually decreases. This spectral change is attributed to the formation of nanodisk arrays. As discussed above, the reduction of nanodisks by 1-DT decreases the hole density, leading to a red-shifted LSPR peak and a weak optical density. In general, the LSPR peak and the extinction intensity of plasmonic NPs are sensitive to the refractive index of the surrounding medium and the type of molecules capping the NPs.[27] These two effects are excluded here, however, because the Cu_7S_4 nanodisks and arrays are both dispersed in $CHCl_3$, and both OAm and 1-DT have essentially the same refractive indexes (1.46, 1.45, respectively).

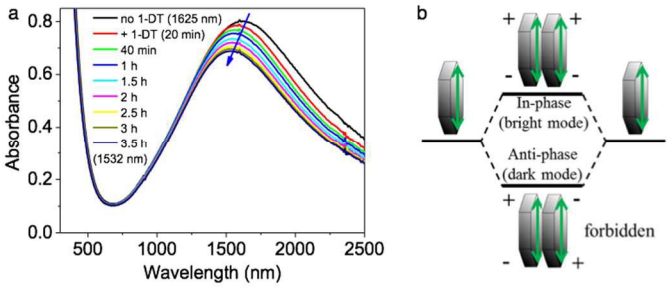

Fig. 4 (a) Time evolution of UV-vis-NIR absorption spectra of oxidized Cu_7S_4 nanodisks in $CHCl_3$ (5 mL) after injection of 1-DT (80 μmol) and sonication under N_2 for 30 min. (b) There are two in-plane plasmon coupling modes for nanodisks assembled in a face-to-face fashion.

Plasmon coupling can be treated much like molecular orbital hybridization. The plasmon mode Ψ_1 in one NP can interact with the plasmon mode Ψ_2 of an adjacent NP, either in-phase ($\Psi_1+\Psi_2$), or anti-phase ($\Psi_1-\Psi_2$). If light is polarized perpendicular to the inter-particle axis (in-plane polarization), the in-phase mode represents anti-bonding (bright mode), which causes a blue shift of the LSPR peak and a decrease in optical density. Conversely, the anti-phase mode represents bonding (dark mode). For a homodimer of NPs, only the in-phase mode is observed under in-plane polarization, while the out-of-phase mode is forbidden because the two dipole moments cancel each other.[28,29] The spectral change of the face-to-face assembled Cu_7S_4 nanodisks in Figure 4a is consistent with this in-phase coupling of the in-plane LSPR mode of the nanodisks (see Figure 4b). Therefore, we conclude that the LSPR peak in the NIR region mainly originates from the in-plane oscillation mode. Furthermore, an increased number of coupled nanodisks in an array results in a larger blue shift of the LSPR peak. A decrease in the absorption intensity results from precipitation of long nanodisk arrays, as well as from plasmon coupling.

For digenite $Cu_{7.2}S_4$ nanodisks, Tao et al. observed two distinct LSPR peaks that were assigned to out-of-plane (NIR region) and in-plane (MIR region) oscillation modes. Whereas, for covellite CuS nanodisks, they observed only one LSPR peak that was assigned to the in-plane oscillation mode (NIR region).[19] Here, roxbyite Cu_7S_4 nanodisks had only one LSPR peak assigned to the in-plane oscillation mode. Thus, the LSPR response of semiconductors can be significantly affected by their crystal structures.[12,13,19]

Length control of Cu_7S_4 nanodisk arrays.

To demonstrate the tunability of in-plane plasmon coupling in Cu_7S_4 nanodisk arrays, the dependence of the LSPR peak shift on 1-DT concentration was investigated. Figure 5a plots the DLS spectra of the Cu_7S_4 nanodisk arrays formed by the addition of different concentrations of 1-DT.

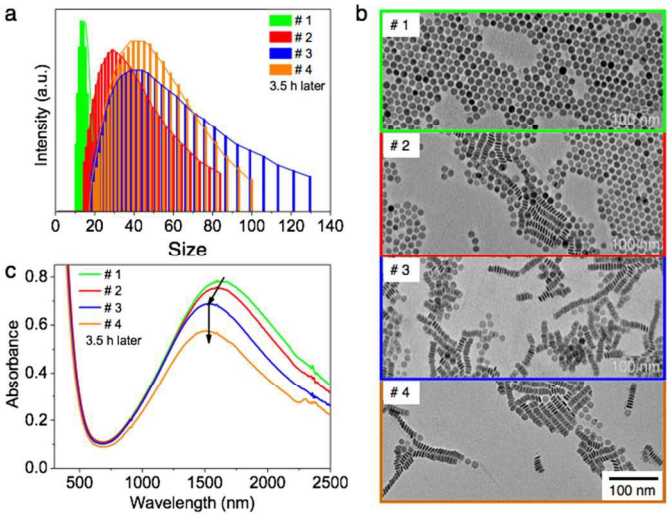

Fig. 5 (a) DLS spectra recorded after the addition of various amounts of 1-DT to oxidized Cu_7S_4 nanodisks in $CHCl_3$ (5 mL), with sonication under N_2 for 30 min. Amounts of 1-DT : # 1: 0.0 μmol, # 2: 10 μmol, # 3: 80 μmol and # 4: 420 μmol, respectively. (b) TEM images and (c) UV-vis-NIR absorption spectra of the corresponding samples.

Low concentrations of 1-DT (# 2, 10 μmol) cause the formation of short nanodisk arrays (15−85 nm); there are also a large number of free Cu_7S_4 nanodisks (Figur 5b). This indicates that the OAm is not completely replaced by the 1-DT. An increase in 1-DT concentration (# 3, 80 μmol) results in longer arrays (18−130 nm), with a smaller number of free nanodisks. For an excess of 1-DT (# 4, 420 μmol), the array distribution is narrower (20−100 nm). The average length of the nanodisk arrays increases to 16 nm with increasing 1-DT concentration. When the amount of 1-DT was sufficient for complete replacement of the OAm, the LSPR shift leveled off. We estimate that 6.3 μmol of 1-DT is necessary to completely

passivate the hexagonal {100} facets of the Cu_7S_4 nanodisks and saturate the growth of the arrays (see ESI and Fig. S6). This fact can be understood in terms of the equilibrium between the adsorption of OAm and 1-DT on the nanodisk surface. Figure 5 plots the UV-vis-NIR absorption spectra of the corresponding samples. As discussed above, in-plane plasmon coupling causes the LSPR blue shift, which is determined by the number of disks in the arrays.

Conclusions

In summary, we synthesized high-quality, OAm capped Cu_7S_4 nanodisks that have a single strong LSPR peak in the NIR region. Cu_7S_4 nanodisk arrays were fabricated *via* ligand exchange and their formation mechanism was investigated. By comparing the LSPR properties of isolated nanodisks with the nanodisk arrays, the singular LSPR peak of roxbyite Cu_7S_4 was assigned, for the first time, to the in-plane oscillation mode. In addition, LSPR spectra of Cu_7S_4 nanodisks can be controlled by the amount of 1-DT because of the variable length of the nanodisk arrays. Our versatile method could provide a way to determine the LSPR oscillation mode of copper-based binary, ternary, and quaternary semiconductors with different crystal structures.

Acknowledgements

This work was supported by the Artificial Photosynthesis Project (ARPChem) of the New Energy and Industrial Technology Development Organization (NEDO) of Japan and JSPS KAKENHI (No. 25390017) (M.S.). We thank Dr. Nakata and Prof. Morii (Institute of Advanced Energy, Kyoto University) for the ^{1}H-NMR measurement. We thank Dr. Sakakibara and Prof. Tsujii (ICR, Kyoto University) for the DLS measurement.

Notes and references

[a] Department of Chemistry, Graduate School of Science, Kyoto University, Gokasho, Uji, Kyoto 611-0011, Japan.
[b] Institute for Chemical Science, Kyoto University, Gokasho, Uji, Kyoto 611-0011, Japan.
[c] PRESTO, Japan Science and Technology Agency, Gokasho, Uji, Kyoto 611-0011, Japan.

Electronic Supplementary Information (ESI) available: [UV-vis-NIR spectra and TEM images of oxidized, reduced and re-oxidized Cu_7S_4 nanodisks, TEM and SEM images of Cu_7S_4 nanodisk arrays, Calculation of the coverage amount of 1-DT]. See DOI: 10.1039/b000000x/

1 S. Linic, P. Christopher and D. B. Ingram, *Nature Mater.*, 2011, **10**, 911.
2 K. L. Kelly, E. Coronado, L. L. Zhao and G. C. Schatz, *J. Phys. Chem. B*, 2003, **107**, 668.
3 X. H. Huang, I. H. El-Sayed, W. Qian and M. A. El-Sayed, *J. Am. Chem. Soc.*, 2006, **128**, 2115.
4 G. Chen, Y. Wang, M. X. Yang, J. Xu, S. J. Goh, M. Pan and H. Y. Chen, *J. Am. Chem. Soc.*, 2010, **132**, 3644.
5 H. Naiki, A. Masuhara, S. Masuo, T. Onodera, H. Kasai and H. Oikawa, *J. Phys. Chem. C*, 2013, **117**, 2455.
6 D. B. Ingram and S. Linic, *J. Am. Chem. Soc.*, 2011, **133**, 5202.
7 J. M. Luther, P. K. Jain, T. Ewer and A. P. Alivisatos, *Nature Mater.*, 2011, **10**, 361.
8 M. Kanehara, H. Koike, T. Yoshinaga and T. Teranishi, *J. Am. Chem. Soc.*, 2009, **131**, 17736.
9 D. J. Rowe, J. S. Jeong, K. A. Mkhoyan and U. R. Kortshagen, *Nano Lett.*, 2013, **13**, 1317.
10 I. Kriegel, C. Y. Jiang, J. Rodríguez-Fernández, R. D. Schaller, D. V. Talapin, E. da Como and J. Feldmann, *J. Am. Chem. Soc.*, 2012, **134**, 1583.
11 D. J. Chakrabarti and D. E. Laughlin, *Bull. Alloy Phase Diagrams*, 1983, **4**, 254.
12 S.-W. Hsu, K. On and A. R. Tao, *J. Am. Chem. Soc.*, 2011, **133**, 19072.
13 Y. Xie, L. Carbone, C. Nobile, V. Grillo, S. D'Agostino, F. D. Sala, C. Giannini, D. Altamura, C. Oelsner, C. Kryschi and P. D. Cozzoli, *ACS Nano*, 2013, **7**, 7352.
14 Y. B. Li, W. Lu, Q. Huang, M. Huang, C. Li and W. Chen, *Nanomedicine*, 2010, **5**, 1161.
15 C. M. Hessel, V. P. Pattani, M. Rasch, M. G. Panthani, B. Koo, J. W. Tunnell and B. A. Korgel, *Nano Lett.*, 2011, **11**, 2560.
16 S. C. Riha, D. C. Johnson and A. L. Prieto, *J. Am. Chem. Soc.*, 2011, **133**, 1383.
17 M. A. Mahmoud and M. A. El-Sayed, *J. Phys. Chem. Lett.*, 2013, **4**, 1541.
18 I. Kriegel, J. Rodríguez-Fernández, A. Wisnet, H. Zhang, C. Waurisch, A. Eychmüller, A. Dubavik, A. O. Govorov and J. Feldmann, *ACS Nano*, 2013, **7**, 4367.
19 S.-W. Hsu, C. Ngo and A. R .Tao, *Nano Lett.*, 2014, **14**, 2372.
20 M. Maillard, S. Giorgio and M. P. Pileni, *J. Phys. Chem. B*, 2003, **107**, 2466.
21 N. J. Nalas, S. Lal, W. S. Chang, S. Link and P. Nordlander, *Chem. Rev.*, 2011, **111**, 3913.
22 M. Kanehara, H. Arakawa, T. Honda, M. Saruyama and T. Teranishi, *Chem. Eur. J.*, 2012, **18**, 9230.
23 P. K. Jain, K. Manthiram, J. H. Engel, S. L. White, J. A. Faucheaux and A. P. Alivisatos, *Angew. Chem. Int. Ed.*, 2013, **52**, 13671.
24 Y. Wu, C. Wadia, W. Ma, B. Sadtler and A. P. Alivisatos, *Nano Lett.*, 2008, **8**, 2551.
25 D. Dorfs, T. Härtling, K. Miszta, N. C. Bigall, M. R. Kim, A. Genovese, A. Falqui, M. Povia and L. Manna, *J. Am. Chem. Soc.*, 2011, **133**, 11175.
26 R. Sato, M. Kanehara and T. Teranishi, *Small*, 2011, **7**, 469.
27 M. A. Mahmoud, M. Chamanzar, A. Adibi and M. A. El-Sayed, *J. Am. Chem. Soc.*, 2012, **134**, 6434.
28 S. Sheikholeslami, Y.-W. Jun, P. K. Jain and A. P. Alivisatos, *Nano Lett.*, 2010, **10**, 2655.
29 P. K. Jain and M. A. El-Sayed, *Chem. Phys. Lett.*, 2010, **487**, 153.